

Shape Evolution and Self Assembly of Monodisperse PbTe Nanocrystals

Weigang Lu,^{†‡} Jiye Fang,^{*†‡} Kevin L. Stokes,^{‡§} and Jun Lin^{||}

Department of Chemistry, AMRI, Department of Physics, University of New Orleans, New Orleans, Louisiana 70148, and Key Laboratory of Rare Earth Chemistry and Physics, Changchun Institute of Applied Chemistry, Chinese Academy of Sciences, Changchun 130022, P.R. China

Received May 25, 2004; E-mail: jfang1@uno.edu

Lead chalcogenides are very promising materials for thermoelectric (TE) applications^{1–3} due to their narrow band gaps and face-centered cubic structure. Both theoretical predictions^{4,5} and MBE experimental exploration^{6,7} suggest that large improvements in figure of merit (ZT) could be achieved in nanostructured systems. It is therefore essential to develop a new approach of fabricating nanophased lead chalcogenides to enhance the TE performance. Actually, it has been demonstrated that high-temperature solution-phase synthesis (HTSPS) is a very promising method to develop monodisperse PbSe⁸ and PbS⁹ nanocrystals (NCs) with size- and shape control. Furthermore, optical studies^{8,10} have suggested that the band gap of PbSe produced in this approach is tunable by controlling the crystalline size, and it is possible to achieve an electrically conductive film of PbSe NCs (a potential nanostructured TE material) after self-assembly and subsequent annealing process.¹¹ Since it was reported that PbTe¹² and PbTe-based compounds¹³ are superior materials for solid-state TE cooling and electrical power generation devices, in this communication we demonstrate our progress in synthesis and self-assembly of PbTe NCs with size- and shape control by employing the HTSPS approach, providing an alternative avenue of preparing PbTe and PbTe-based NCs for further TE manipulation.

Basically, high-quality spherical PbTe NCs were synthesized by rapidly injecting a cold solution (~ 10 °C) of lead acetate trihydrate and trioctylphosphine telluride (TOP-Te) into vigorously stirring hot phenyl ether, in the presence of oleic acid, at 200 °C in a three-neck flask equipped with a condenser under an argon stream. Upon injection, small PbTe clusters nucleated and started to grow with stabilization provided by the capping ligands (TOP and oleic acid), forming spherical PbTe nanocrystals in ~ 5 min. Extending the growth time results in a further development of the PbTe crystalline morphology. When they were aged for ~ 25 min, cubic PbTe NCs could be achieved. The posttreatment of a size-selective precipitation is essential in further refining the size distribution for both types of NCs. The details of the preparation procedure can be found in Supporting Information (SI). PbTe NCs were stored in hexane after the posttreatment and were self-assembled on TEM grids and on the surface of single-crystalline Si wafers for morphological characterization using a transmission electron microscope (TEM, JEOL2100) and for phase identification using an X-ray diffractometer (XRD, Philips X-pert system), respectively.

The self assembly of spherical PbTe NCs was carried out from a mixed solvent of hexane and hexanol on to a TEM grid. Figure 1a demonstrates a TEM image of hexagonally ordered, monolayer-assembled PbTe pattern, showing a spherical morphology with an average diameter of $\sim 8 \pm 1.6$ nm. The standard deviation of

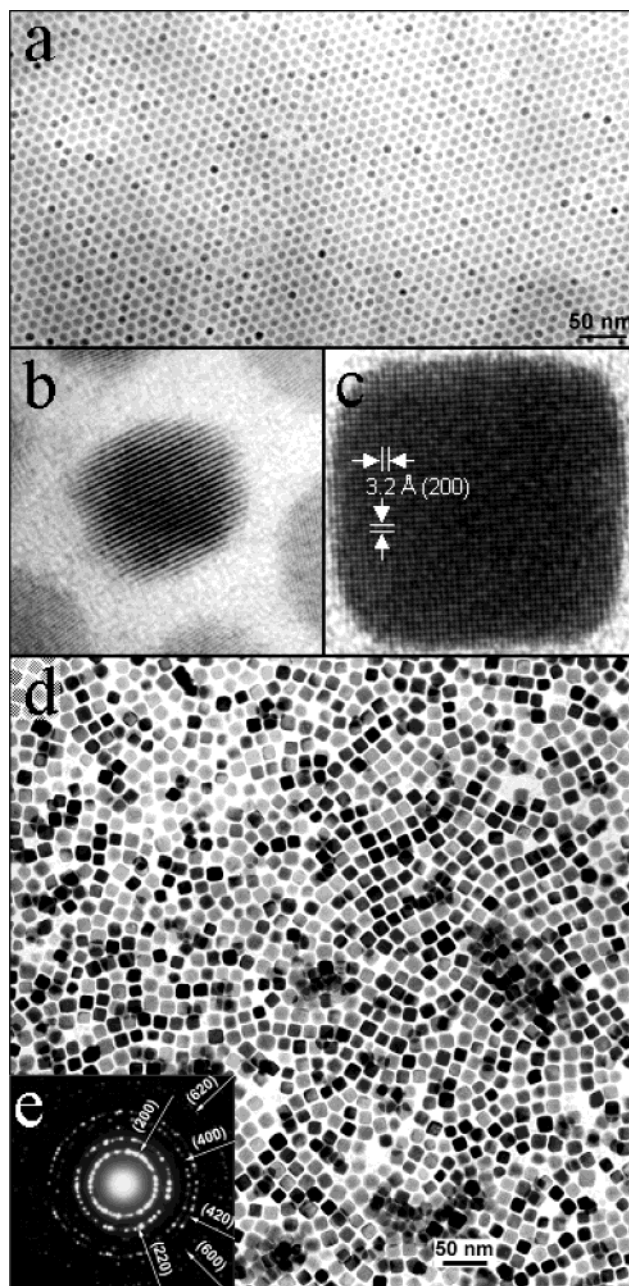


Figure 1. (a) Transmission electron micrograph (TEM) image of spherical PbTe NCs (monolayer assembly); (b) HRTEM of a spherical PbTe NC; (c) HRTEM of a cubic PbTe NC; (d) TEM image of cubic PbTe NCs (monolayer assembly); (e) SAED of cubic PbTe NCs (~ 40 NCs).

crystalline size was calculated as $\delta \leq \sim 7\%$ based on the size distribution (in hexane) of PbTe NCs measured by using a light-

[†] Department of Chemistry, University of New Orleans.

[‡] AMRI, University of New Orleans.

[§] Department of Physics, University of New Orleans.

^{||} Key Laboratory of Rare Earth Chemistry and Physics, Changchun Institute of Applied Chemistry, Chinese Academy of Sciences.

scattering technique (see Figure S1a in SI). The minimum spacing between NCs is approximately 2.5 nm and uniform. Figure 1b reveals a high-resolution TEM image (HRTEM) of a single PbTe NC, indicating its high crystallinity. We further extended the growth time using a similar preparation procedure to investigate the shape evolution of these PbTe NCs. Figure 1d is a typical TEM image of the cubic PbTe NC's self-assembled pattern, in which locally ordered and monodisperse NCs with an average size of $\sim 14 \pm 1.2$ nm can be detected. The size distribution was also calculated as $\delta \leq \sim 6\%$ based on the light-scattering study (see Figure S1b in SI). To determine the accurate structure of this sample, the TEM-selected area electron diffraction (SAED) pattern of more than 40 NCs was recorded as shown in Figure 1e (as well as in Figure S2 in SI). From this SAED pattern, all the detectable dot-rings are perfectly indexed to the same positions as those from fcc standard bulk PbTe.¹⁴ Furthermore, Figure 1c gives a projected profile of HRTEM image on a cubic PbTe NC oriented along $\langle 100 \rangle$. The distances between the adjacent lattice fringes, measured as 3.2 Å, are the interplanar distances of PbTe (200), which are in excellent agreement with the (200) d spacing of the fcc literature value,¹⁴ 3.23 Å.

It is generally believed that, for a spherical single-phase crystal with a size smaller than 10–20 nm, its surface must be a polyhedron containing high-index crystallography planes¹⁵ which possibly result in a higher surface energy. Actually, the intrinsic properties of surface energy are very important to nanocrystalline growth rate. The growth rates on different surface facets are dominated by the surface energy. When a particle grows, facets tend to form on the low-index planes to minimize the surface energy. Traditionally, the shape of an fcc NC is determined by the ratio, R , of the growth rate in the $\langle 100 \rangle$ directions to that of the $\langle 111 \rangle$ directions.^{15,16} In the case of nanocrystalline rock salts, $\{111\}$ crystallographic facets have higher surface energy than that of $\{100\}$ planes.¹⁷ Once the NC formation is initiated by an injection, R should be achieved with a high value. Because the $\{111\}$ facets are high-index planes in comparison with the $\{100\}$ facets, the $\{100\}$ facets will develop to increase the portion of low energetic surface, and the R will therefore be reduced from 1.73 as the growth time increases. This results in truncated octahedral shapes ($0.87 < R < 1.73$) for the particles. The existence of these truncated octahedral particles can be verified by the projected profile of TEM image on a sample which was extracted at 10 min, before the perfect cubic NCs were completely developed (see Figure S3 in SI). When this high-temperature growth is kept for a long enough time, perfect cubes (R approaches 0.58) bound by $\{100\}$ planes (which possess relatively lower energy in comparison with those of $\{111\}$ surfaces) result. Under the current experimental conditions, in other words, we can control the PbTe shape-evolution by simply tuning the growth time. The time for achieving the smallest R (0.58, cubic NCs) is roughly 25 min in our investigation.

Both spherical NCs and cubic NCs were also self-assembled on single-crystalline silicon wafers for powder XRD characterization. Figure 2(a,b) presents the XRD patterns recorded on these two samples, indicating that both types of NCs are well-defined fcc structure with the $Fm\bar{3}m$ space group ($a = 6.459$ Å).¹⁴ For a comparison, the relative intensities of the diffraction peaks from the standard card¹⁴ were labeled on the bottom of Figure 2 as well. By applying the Scherrer equation¹⁸ to the line broadening of the (200) peak, the crystalline sizes were estimated¹⁹ as 7.4 and 13 nm for spherical and cubic particles, respectively, which are consistent with the results from TEM observation. It is worth noting that for the cubic NCs the diffraction peaks (200) and (400) dominate the pattern. The relative intensity enhancement on peaks (200) and (400) indicates that only the (200) [and (400)] facets (see Figure 1c) have

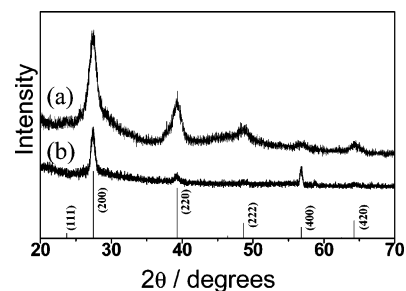


Figure 2. X-ray powder diffraction patterns of (a) spherical PbTe NC (8 nm in diameter) assembly on Si wafer; (b) cubic PbTe NC (14 nm in size) assembly on Si wafer.

a chance to be diffracted (note that the diffraction plane in XRD is different from the plane in TEM), further confirming that these NCs assembled on surface of the Si wafer are perfect cubes. This observation suggests that it is possible to chemically achieve a $\{200\}$ -perfect-orientated monolayer of PbTe assembly with nanocubes.

In conclusion, we have demonstrated the synthesis and self assembly of both spherical and perfect cubic PbTe NCs using an HTSPS approach. The mechanism of nanocrystalline evolution from spherical to cubic structure has also been discussed. It is possible to employ these highly orientated PbTe NCs as building blocks to achieve thickness-controlled film for further manipulations into thermoelectric devices.

Acknowledgment. This work was supported by DARPA through ONR N00014-02-1-0729, LEQSF(2002-05)-RD-B-15, and NSF/LA-BoR (2001-04)-RII-03. Prof. Fang is grateful for the financial support by two-base program for international cooperation of NSFC related to the project 50225205 of Prof. Lin. We also thank Drs. Jinke Tang, Yuxi Chen, and Wendong Wang for their help in providing the XRD device, TEM observation, and discussion of the crystalline structure, respectively.

Supporting Information Available: Size distribution, SAED, and TEM image (truncated octahedral PbTe NCs). This material is available free of charge via the Internet at <http://pubs.acs.org>.

References

- (1) Shchennikov, V. V.; Ovsyannikov, S. V. *Solid State Commun.* **2004**, *126*, 373–378.
- (2) Ovsyannikov, S. V.; Shchennikov, V. V.; Ponosov, Y. S.; Gudina, S. V.; Guk, V. G.; Skipetrov, E. P.; Mogilenskikh, V. E. *J. Phys. D: Appl. Phys.* **2004**, *37*, 1151–1157.
- (3) Chung, D.-Y.; Iordanidis, L.; Choi, K.-S.; Kanatzidis, M. G. *B Korean Chem. Soc.* **1998**, *19*, 1283–1293.
- (4) Hicks, L. D.; Dresselhaus, M. S. *Phys. Rev. B* **1993**, *47*, 12727–12731.
- (5) Hicks, L. D.; Dresselhaus, M. S. *Phys. Rev. B* **1993**, *47*, 16631–16634.
- (6) Harman, T. C.; Taylor, P. J.; Spears, D. L.; Walsh, M. P. *J. Electron. Mater.* **2000**, *29*, L1–L4.
- (7) Hicks, L. D.; Harman, T. C.; Sun, X.; Dresselhaus, M. S. *Phys. Rev. B* **1996**, *53*, R10493–R10496.
- (8) Murray, C. B.; Sun, S.; Gaschler, W.; Doyle, H.; Betley, T. A.; Kagan, C. R. *IBM J. Res. Dev.* **2001**, *45*, 47–56.
- (9) Lee, S.-M.; Jun, Y.-w.; Cho, S.-N.; Cheon, J. *J. Am. Chem. Soc.* **2002**, *124*, 11244–11245.
- (10) Du, H.; Chen, C.; Krishnan, R.; Krauss, T. D.; Harbold, J. M.; Wise, F. W.; Thomas, M. G.; Silcox, J. *Nano Lett.* **2002**, *2*, 1321–1324.
- (11) Chen, F.; Stokes, K. L.; Zhou, W.; Fang, J.; Murray, C. B. *Mater. Res. Soc. Symp. Proc.* **2002**, *691*, 359–364.
- (12) Harman, T. C.; Taylor, P. J.; Walsh, M. P.; LaForge, B. E. *Science* **2002**, *297*, 2229–2232.
- (13) Hsu, K. F.; Loo, S.; Guo, F.; Chen, W.; Dyck, J. S.; Uher, C.; Hogan, T.; Polychroniadis, E. K.; Kanatzidis, M. G. *Science* **2004**, *303*, 818–821.
- (14) JCPDS-ICDD card 38-1435.
- (15) Wang, Z. L. *J. Phys. Chem. B* **2000**, *104*, 1153–1175.
- (16) Sun, Y.; Xia, Y. *Science* **2002**, *298*, 2176–2179.
- (17) Lee, S.-M.; Cho, S.-N.; Cheon, J. *Adv. Mater.* **2003**, *15*, 441–444.
- (18) Cullity, B. D. *Elements of X-ray Diffraction*, 2nd ed.; Addison-Wesley: Reading, Massachusetts, 1978.
- (19) Fang, J.; Stokes, K. L.; Wiemann, J. A.; Zhou, W.; Dai, J.; Chen, F.; O'Connor, C. J. *Mater. Sci. Eng., B* **2001**, *83*, 254–257.

JA0469131